Corrosion Behaviour of Ti–34Nb–25Zr Alloy Fabricated by Spark Plasma Sintering

M. R. Mahundla[1] · W. R. Matizamhuka[1] · A. Yamamoto[2] · M. B. Shongwe[3] · R. Machaka[4]

Abstract

Titanium alloys are often used in orthopaedic applications owing to their superior mechanical properties and corrosion resistance. Passive corrosion or material degradation process such as wear has been reported due to the release of titanium and other alloying elements into the surrounding tissue. It is therefore important to study the corrosion behaviour of the alloy in biomedical environments. A sub-micron grain-structured Ti–34Nb–25Zr (TNZ) alloy was fabricated via mechanical alloying (MA) of elementary powders followed by spark plasma sintering (SPS). The electrochemical behaviour of TNZ alloy was investigated at 37 °C for 4 h in three different solutions; the Hank's, the 0.9 wt% NaCl and the eagle minimum essential medium + 10% fetal bovine serum (E-MEM + 10%FBS) solutions. The results show E_{corr} values for TNZ alloy in Hank's, 0.9 wt% NaCl and E-MEM + 10%FBS solutions were about − 202 mV, − 251 mV and − 171 mV, respectively. The measured i_{corr} values were ~ 1.66 nA/cm^2 in hank's solution, which is lower than that in 0.9 wt% NaCl (~ 4.20 nA/cm^2) and E-MEM + 10% FBS solution (~ 3.19 nA/cm^2). TNZ exhibits good corrosion resistance in all the solutions.

Keywords Corrosion · Spark plasma sintering · E-MEM · Potentiodynamic polarisation · FBS

1 Introduction

Biometallic materials are being increasingly used in medical applications as implants [1]. Titanium alloys are the mostly used metallic biomaterials, specifically for biomedical applications [2]. They possess a set of suitable properties such as low specific weight, high corrosion resistance and biocompatibility [3]. Corrosion resistance is a property of utmost importance in biomedical applications [4]. Biomedical implants are subjected to physiological fluids which contain chloride ions

✉ M. R. Mahundla
mahundla.mr@gmail.com

1   Department of Metallurgical Engineering, Vaal University of Technology, Andries Potgieter Blvd, Private Bag X021, Vanderbijlpark, South Africa

2   National Institute for Materials Science, 1-1 Namiki, Tsukuba, Ibaraki 305-0044, Japan

3   Tshwane University of Technology, Staatstirstille Road, Pretoria, South Africa

4   Titanium Centre of Competence, Materials Science & Manufacturing, Council for Scientific and Industrial Research, Meiring Naudé Road, Brummeria, Pretoria 0185, South Africa

and maintained at 37 °C. In addition, if corrosion products are formed, they result in limited biocompatibility and may produce undesirable reactions in implant-adjacent tissues [5], and corrosion resistance helps in deciding whether the alloy is a best candidate for use as a biomaterial. Electrochemical corrosion study by Saji and Choe showed that the nanotubular alloy of Ti-13Nb-13Zr possesses lower corrosion resistance properties. The higher corrosion current density obtained for the nanotubular alloy (2.04 µA/cm^2) [6]. According to the study by Wang and Zheng, the passivation current density is among 4.16–5.72 µA/cm^2 for Ti–16Nb alloy and 5.67–7.8 µA/cm^2 for CPTi, and the repassivation current density is among 12.1–13.4 µA/cm^2 for Ti–16Nb alloy and 18.2–20 µA/cm^2 for CP Ti in Hank's solution. The corrosion potential (E_{corr}) and the corrosion current density (i_{corr}) of Ti–16Nb sample had lower I_{corr} (3.557($\pm$ 1.281) × 10^{-3} µA/cm^2) and lower E_{corr} (− 0.403 ± 0.020 V), in comparison with CP Ti (E_{corr} = − 0.341 ± 0.020 V] i_{corr} = 7.616(± 0.145) × 10^{-2} µA/cm^2) [7]. The values of the studied alloys were the benchmarking E_{corr} and I_{corr} values for Cp Ti and Ti–6Al–4V (Ti-64) for the current study.

Ti-64 was the first titanium alloy used for implant materials, and Ti-64 is one of the most used implant materials for dental, orthopaedic and osteosynthesis applications [8]. However,

studies have indicated that vanadium, a beta-phase stabilizer, produces oxides harmful to the human body [8, 9]. The toxicity of vanadium has encouraged the search for alternative materials to replace Ti-64 [9].

All the three constituents in the Ti–Nb–Zr alloy meet the criteria for biomaterials in terms of biocompatibility, resistance to corrosion, mechanical considerations and ionic cytotoxicity [5]. The addition of Nb to Ti alloys stabilizes the β phase and possesses improved mechanical properties. This results in improved wear resistance, while the addition of Zr helps in obtaining the solid solution required for achieving the hardness [2]. Most of the work in literature on the development of Ti-based alloys use arc melting and casting techniques [2, 3, 6–13]. However, owing to the broad range of melting temperatures in most of these alloys, the use of conventional casting methods becomes limited owing to the lack of homogeneity in the final product [2]. Powder metallurgy (PM) processing provides an alternative route for the synthesis of Ti-based alloys consisting of elements with a wide range of melting temperatures. Owing to solid-state processing in PM process, more homogenous alloys are expected to be produced compared to other techniques, especially when the alloying element has a higher melting temperature such as Nb [4].

Ozan et al., developed Ti–34Nb–25Zr (TNZ) alloy with considerable plastic deformation ability during compression test, high elastic admissible strain and excellent cytocompatibility for removable bone tissue implant applications. TNZ alloy was fabricated using the cold-crucible levitation technique, and the effects of alloying element content on their microstructures, mechanical properties (tensile strength, yield strength, compressive yield strength, Young's modulus, elastic energy, toughness and micro-hardness) and biocompatibilities were investigated and compared [14]. Ti and Ti-64 have been produced by SPS and their corrosion behaviours were studied and showed nobler i_{corr} values. However, for the TNZ, there is no study showing the corrosion behaviour in simulated body solutions. Biomaterials are also expected to be corrosion resistant since they are exposed to physiological fluids in a human body. Hence, corrosion resistance is of utmost importance in biomaterials. The objective of this study is to evaluate the electrochemical behaviour of TNZ in Hank's, NaCl and eagle minimum essential medium + 10% fetal bovine serum (E-MEM + 10%FBS) solutions in comparison with Ti and Ti-64. The study was carried out using simulated body solutions inside a 37 °C incubator to mimic the human body. Hank's, 0.9 wt% NaCl and E-MEM + 10%FBS solution (the simulated body fluids) were used for the corrosion analysis.

2 Experimental Methods

2.1 Material Preparation and Microstructural Characterization

Elemental powders of titanium, niobium supplied by Alfar Aesar and zirconium supplied by Sigma-Aldrich were used as starting materials. The as-received powders had a purity of 99.8% (Ti, Nb and Zr). The powders of Ti, Nb and Zr were mixed in the ratio of 34 wt% Nb and 25 wt% Zr (balance Ti) in a turbula mixer (WAB, Schatz Willy, A Bachofen, Switzerland). TNZ mixtures were loaded into a zirconia (ZrO_2) vial with ZrO_2 grinding balls of 3 mm in diameter, with 1:10 ball-to-powder ratio. The ternary mixture of the powder was mechanically alloyed (MA) in a high-energy ball mill (Simoloyer high-energy mill, CM-01) at a rotational speed of 500 rpm for 5 h. The as-received and milled powders, and TNZ samples after polarization measurements were characterized by a field emission Scanning electron microscope (FE-SEM) (JEOL SEM, JSM 6510) coupled with Energy dispersive X-ray spectroscopy. The morphology and elemental compositions with the XRD patterns of the starting powders are presented in Fig. 1.

The mechanically alloyed powders were consolidated using a spark plasma sintering (SPS) machine (FCT-systeme-GmbH-model HHPD-25, Germany). The 5 h mechanically alloyed powders were poured into a 40-mm-diameter graphite die. The die was lined inside with a graphite foil to facilitate ease of sample removal after sintering and to reduce friction between the die surface and the powder. The powders were sintered at a temperature of 1200 °C in a vacuum at a pressure of 50 MPa, a heating rate and holding time of 100 °C/min and 10 min, respectively. The temperature of the sintered material was measured by a thermocouple inserted in the die.

The temperature profiles of the sintered Ti, Ti-64 and TNZ are shown in Fig. 2. Pure Ti, Ti-64 alloys were sintered at a temperature of 1200 °C, pressure of 50 MPa, heating rate of 100 °C/min and 10 min, respectively. Temperature measurement on the thermocouple started at 250 °C. However, a time lag difference of about 2 min was noticed between the Ti and Ti-64 specimens during the sintering, as indicated by the blue and green lines in Fig. 2. Although the sintering rate was constant, Ti-64 attained the set sintering temperature (1200 °C) in a shorter time than Ti and TNZ. Ti–34Nb–Zr had a time lag of 10 min during sintering as indicted by the orange line. This difference in thermal response of the different powder compositions can be attributed to the specific heat capacities of the different alloying elements.

The sintered specimens were sand blasted in order to remove the graphitic layer on the surface. The relative

(a)   **(b)**   **(c)**

(d)
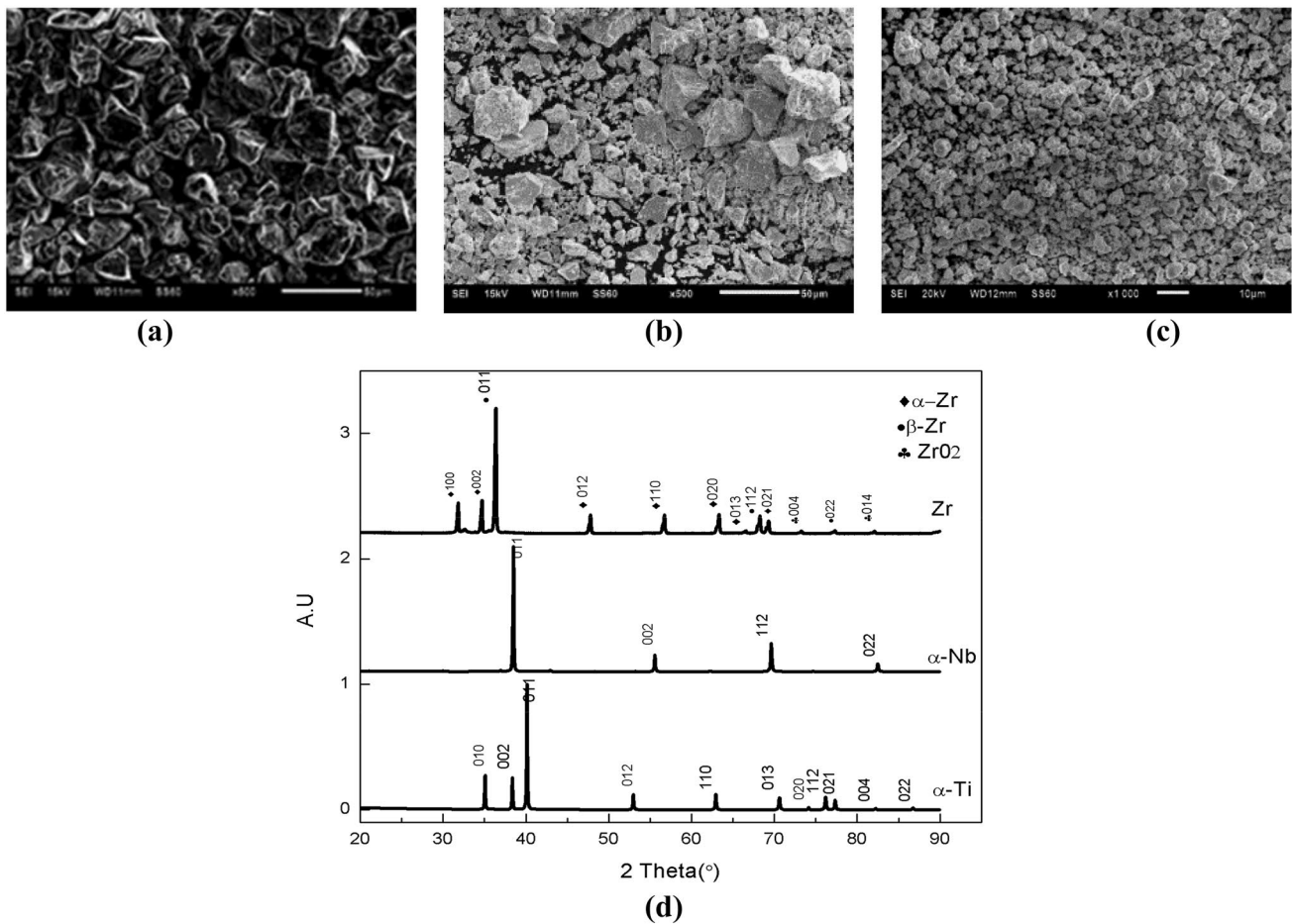
Fig. 1 The as-received powders SEM morphologies of **a** Ti, **b** Nb, **c** Zr and **d** respective XRD patterns
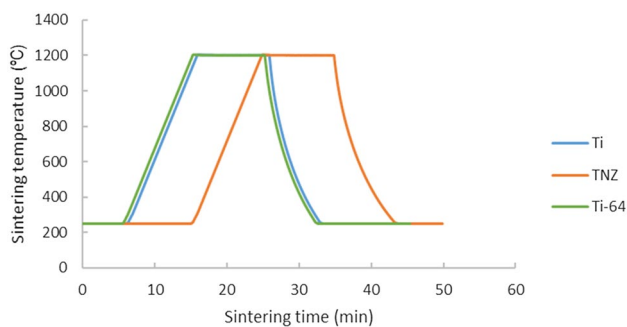
Fig. 2 Temperature profiles of the sintered Ti, Ti-64 and TNZ

density of the sintered specimen was measured according to Archimedes principle at room temperature. The relative density was calculated with reference to the theoretical density using rule of mixtures. The sintered samples were sectioned with a diamond blade and metallographically prepared for phase, microstructural and chemical composition and corrosion analysis. SiC papers were used for the first and final stages of grinding consecutively from #320 down to #600 grit, then polished with 9, 3 μm diamond paste and finally polished to mirror finish surface in 5:2 ratio of colloidal silica and hydrogen peroxide. The polished samples were ultrasonically cleaned for 5 min in acetone, rinsed with ethanol and left to dry in air. A field emission Scanning electron microscope (FE-SEM) (JEOL SEM, JSM 6510) coupled with Energy dispersive X-ray spectroscopy was used to examine the microstructures of the as-received and blended powders.

2.2 Electrochemical Analysis

Electrochemical measurements were conducted using a Potentiostat (VersaStat3, Japan) controlled from a coupled computer. The electrochemical cell was set up inside a ventilated cabinet and placed inside a humidified CO_2 incubator at 37 °C. The electrochemical cell and the chamber inside the incubator are shown in Fig. 3.

Hank's solution, 0.9 wt% NaCl solution and eagle minimum essential medium with 10% fetal bovine serum

Fig. 3 Schematic of the electro-chemical cell and the chamber
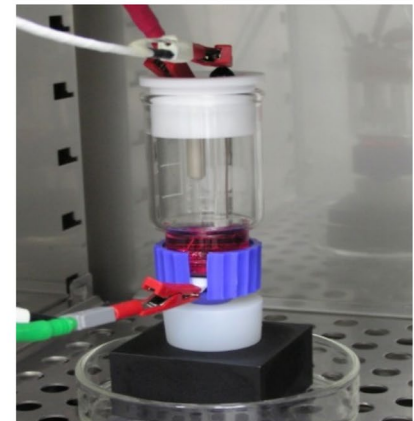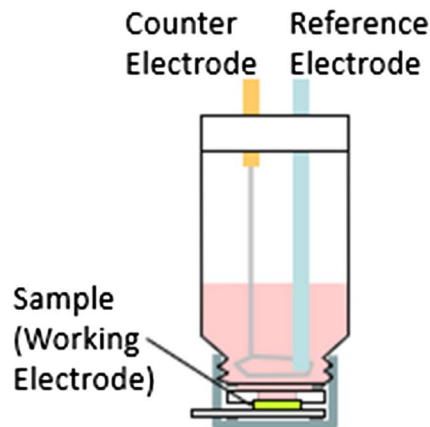
(E-MEM + 10%FBS) were used as corrosion media. The Ti, Ti-64 and TNZ samples were set as the working electrodes (WE), in separate experimental set-up. A platinum wire mesh was used as a counter electrode (CE), and a silver–silver chloride (Ag/AgCl in 3 M NaCl) electrode was used as the reference electrode (RE). The standard electrode (SE) was connected to the working electrode.

The sample disk was immersed in 10 ml of Hank's solution with a pH value of 7.4 for 4 h in a humidified 5vol% CO_2 incubator at 37 °C. The exposed sample surface area was 0.899 cm². Open circuit potential (OCP) and potentiodynamic polarization scans were measured after immersion. OCP was measured for 1800 s. Potentiodynamic polarization scans were carried out at a rate of 0.16666 mV/s in the range of − 0.25 (vs OC) to 1.5 mV (vs Ref) after dipping the sample into a corresponding electrolyte for 3.5 h. The current limit was set to be greater or equal to 0.001 μA. The measurements were carried out using a VersoStat3, Potentiostat, Japan. The sample disk was immersed in 10 ml of 0.9 wt% NaCl solution under same conditions as for Hank's solution.

The sample disk was immersed in 10 ml of E-MEM + 10%FBS for 4 h in a humidified 5 vol% CO_2 and 5vol.% O_2 incubator at 37 °C. Open circuit potential (OCP) and potentiodynamic polarization scans were measured after immersion. OCP was measured for 2700 s in order to stabilize the level of CO_2 and O_2 to 5 vol% inside the incubator before potentiodynamic scans were carried out. Tafel extrapolation curves were extracted after the experiment and analysed in order to determine the corrosion rates from the software-based approximations.

2.3 Statistical Analysis

Statistical analysis was done using the independent T test method to evaluate the differences between groups. The significance level of $p < 0.05$ was a significant statistical difference.

3 Results and Discussion

3.1 Microstructural Characterization

The as-received powder morphologies are presented in Fig. 1a–c and their XRD patterns in Fig. 1d. Ti is irregularly
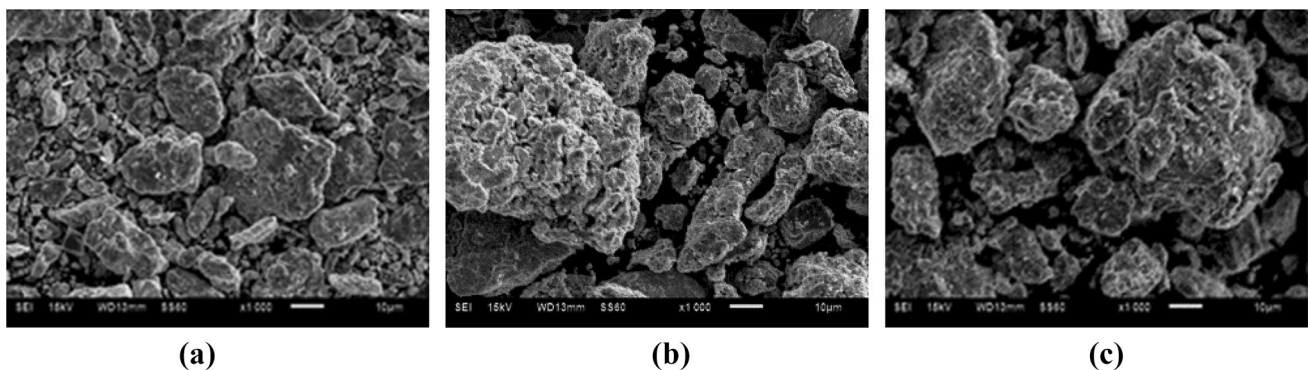
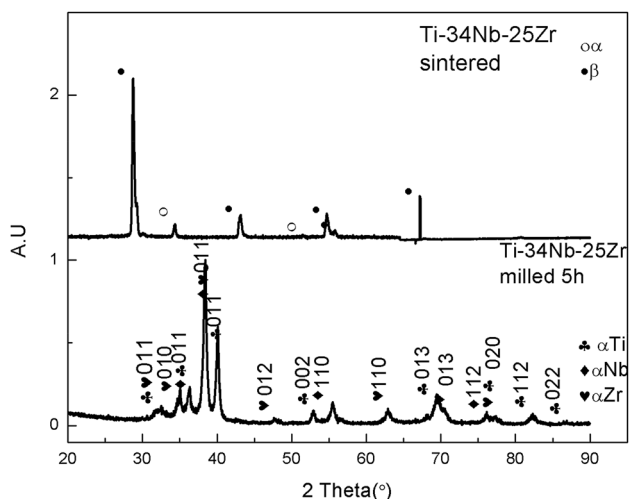**Fig. 4** SEM images of TNZ milled for **a** 1 h, **b** 3 h, and **c** 5 h

Fig. 5 XRD pattern of 5 h milled and sintered TNZ

shaped and nonporous and has a fairly large particle size of − 45 μm (Fig. 1a). Nb powder has an irregular shape and a particle size of 1–5 μm (Fig. 1b), whereas the particle size of Zr is − 90 μm and it is irregularly shaped. The XRD phase analysis of the as-received Ti powder reveals peaks of α-Ti, Nb powder reveals peaks of α-Nb, whereas Zr powder has peaks of two different phases; α-Zr, β-Zr.

Figure 4 shows the morphology of the powder after mechanical alloying for 1, 3 and 5 h, respectively. The milled powders are more agglomerated when compared to the starting powders. The large particles have been attributed to finer particle agglomeration and excessive repeated cold welding [1]. Figure 5 shows XRD patterns of both milled (mechanically alloyed powder) for 5 h and sintered TNZ. It can be clearly seen that the intensity of the diffraction peaks decreased, and the peak width broadening after mechanical alloying for 5 h. The slight peak broadening is due to
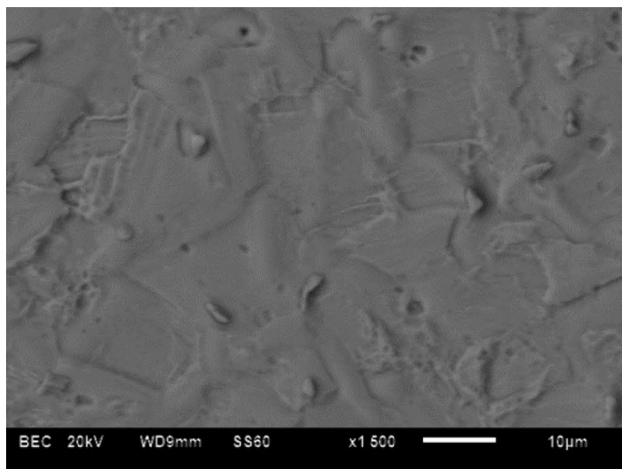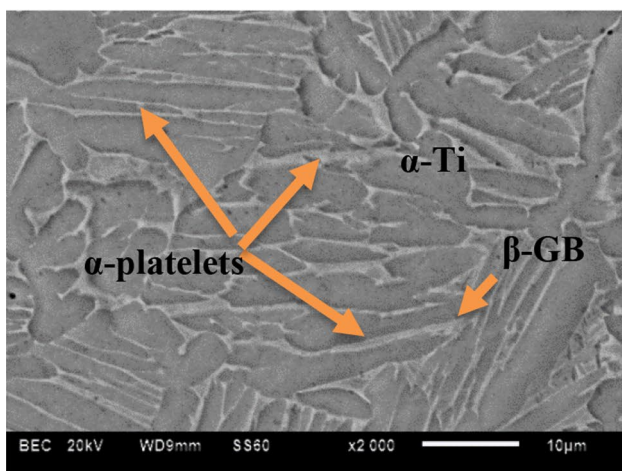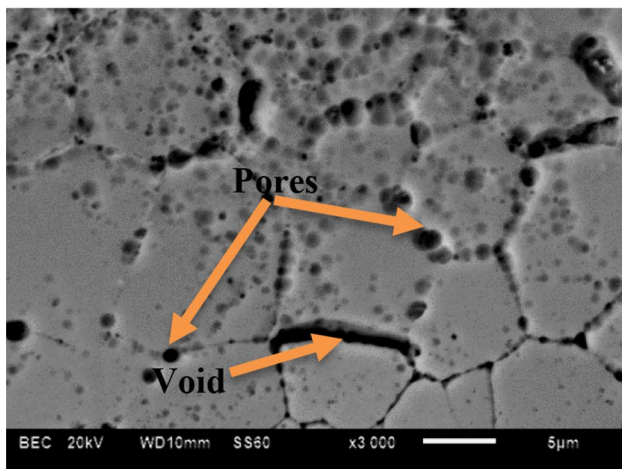

(a) Ti

(b) Nb

(c) Zr
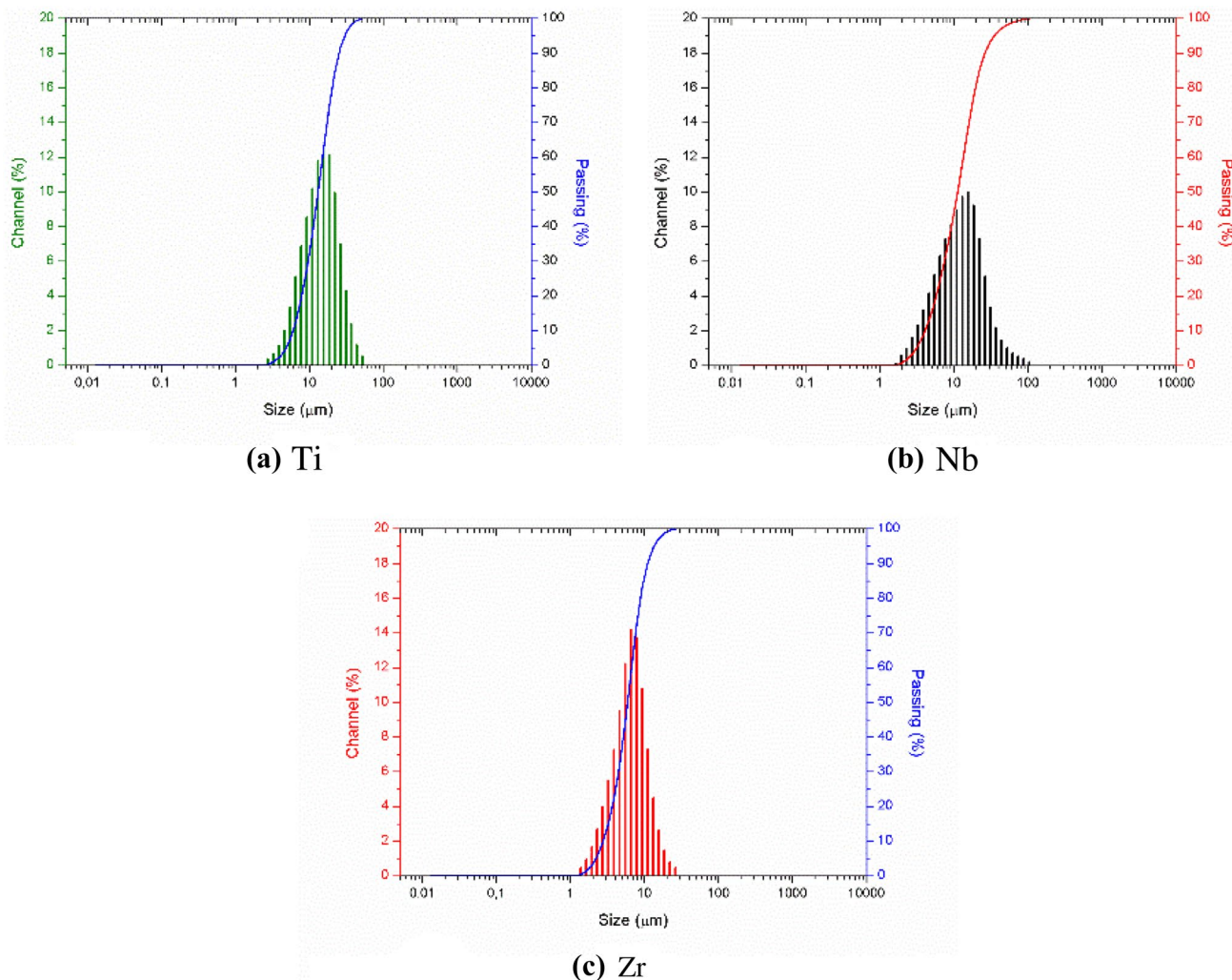
Fig. 6 PSD analysis of the as-received **a** Ti, **b** Nb and **c** Zr

Fig. 7 SEM images **a** Ti, **b** Ti-64 and **c** TNZ
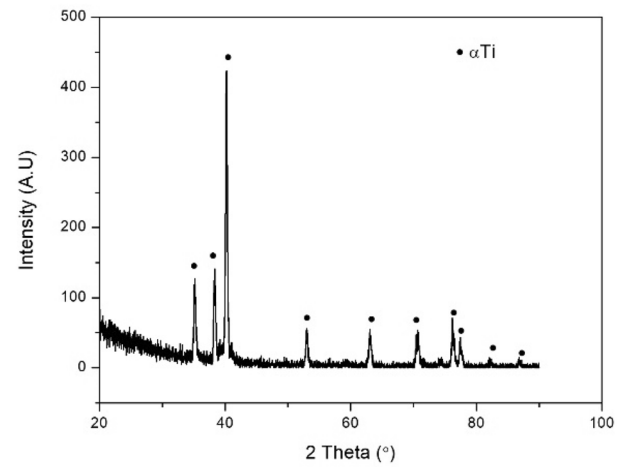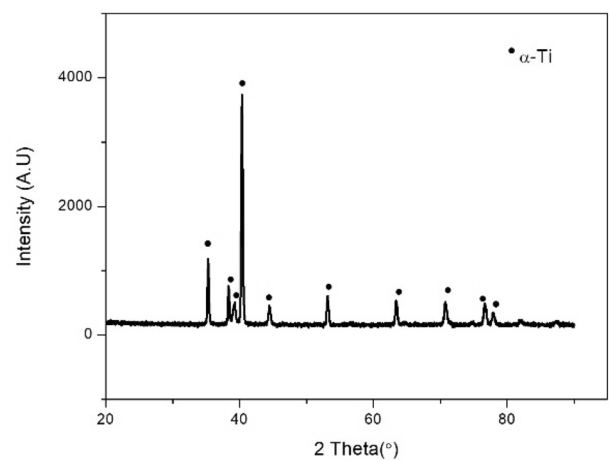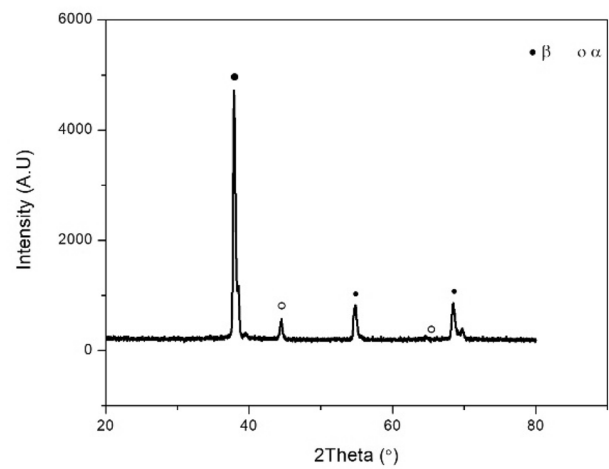
Fig. 8 XRD patterns of the sintered **a** Ti, **b** Ti-64 and **c** TNZ

(a) Hank's solution

(b) 0.9 wt.% NaCl solution

(c) E-MEM +10% FBS solution
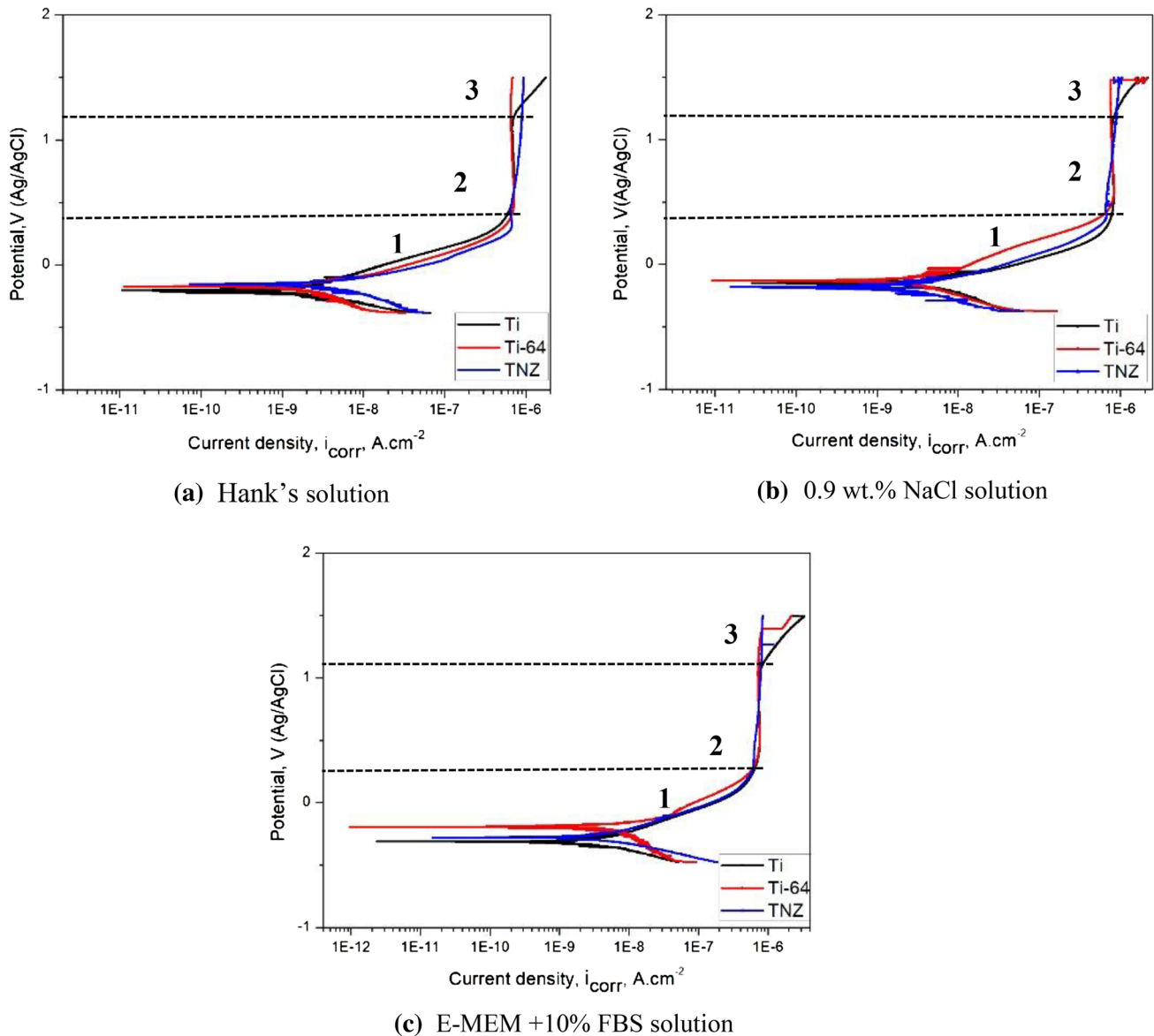
Fig. 9 Potentiodynamic polarization curves of the sintered Ti, Ti-64 and TNZ in **a** Hank's, **b** 0.9 wt% NaCl and **c** E-MEM + 10%FBS solution

grain refinement and plastic deformation, which signifies substantial size reduction. This could also be due to structure distortions and introduction of atoms/defects in vacancies [3]. The intensity of the peaks of beta phase is higher than that of alpha phase. The sample revealed peaks of β-Ti and α orthorhombic martensitic phase. Figure 6 shows the particle size (PSD) analysis of the as-received powders.

3.2 Sintering

The as-received powders SEM morphologies of (a) Ti, (b) Nb, (c) Zr and (d) respective XRD patterns. Figure 7 presents the microstructures of Ti, Ti-64 and TNZ alloy after sintering at 1200 °C at a heating rate and holding time of 100 °C/min and 10 min, respectively. The pure titanium alloy microstructure (Fig. 7a) shows alpha titanium only. The microstructure of Ti-64 (Fig. 7b) consists mainly of equiaxed grains, which contain fine interlocked α platelets (light phase) in a matrix of the primary β-Ti phase (dark phase). The original α phase microstructure changed to α + β structure (which resembles almost the basket-weave structure). The equiaxed gains are separated by a network of the grain boundary αTi phase. The microstructure of TNZ shows a mixture of large and small pores and the grains appear to have voids (Fig. 7c). Figure 8 shows the supporting XRD patterns of the sintered alloys at 1200 °C.

Table 1 Average values of E_{corr} and i_{corr} determined for TNZ alloy from the polarization curves obtained in Hank's, 0.9 wt% NaCl and E-MEM + 10%FBS solutions at 37 °C

Alloy	E_{corr} (mV)	i_{corr} (nA/cm^2)
Hank's solution		
Ti	− 355 ± 5.1	2.03 ± 1
Ti-64	− 272 ± 9	1.99 ± 1
TNZ	− 202 ± 12	1.66 ± 1.5
0.9 wt% NaCl solution		
Ti	− 293 ± 20	4.02 ± 0.1
Ti-64	− 177 ± 11	3.81 ± 2.4
TNZ	− 251 ± 8	4.20 ± 2
E-MEM + 10%FBS solution		
Ti	− 170 ± 6.5	4.20 ± 3
Ti-64	− 112 ± 1	2.45 ± 1
TNZ	− 171 ± 2.5	3.19 ± 1

3.3 Potentiodynamic Polarization Curves

Figure 9 compares typical potentiodynamic polarization curves of the Ti, Ti–6Al–4 and TNZ alloys tested in Hank's solution, 0.9 wt% NaCl and E-MEM + 10%FBS solution at 37 °C after 4 h immersion. The electrochemical behaviour was studied to compare the corrosion resistance Ti-34Nb-2Zr with the benchmarks (Ti and Ti-64). The electrochemical parameters (E_{corr} and i_{corr}) extracted from the Tafel extrapolations using software-based approximations are shown in Table 1.

Figure 10 shows the SEM morphologies of TNZ samples after polarization measurements in Hank's, 0.9 wt% NaCl and E-MEM solution. The sample surfaces are covered with a passive oxide layer with no evidence of obvious pitting corrosion.

3.4 Microstructural Analysis

The microstructure displays a morphology of two phase consisting of β phase grains and α phase precipitated in β matrix. The microstructure shows a lot of pores which may be a result of poor densification although densities of between 97 and 100% were obtained. There are regions in the microstructure that are Zr rich. The Nb- and Zr-rich regions improve the corrosion resistance of materials by the formation of oxides which render the material passive, thereby forming a passive oxide layer.

3.5 Corrosion Behaviour of the TNZ Alloy

The alloy exhibits a typical activation polarization behaviour in both solutions and show a well-defined linear relationship between the potential and the current density in the Tafel regions in comparison to the benchmarks. The corrosion potentials (E_{corr}) and corrosion current densities (I_{corr}) were obtained by Tafel extrapolation analysis using both anodic and cathodic branches of the curves as depicted in Table 1. The current density increased with increasing the potential (region 1) where metal oxidation is the dominant reaction as depicted in Fig. 9. The current densities of the alloy remain very stable in a wide passive region of 500 mV to 1500 mV (vs Ag/AgCl) (Region 2). The very low current densities (order of 10^{-9} A/cm^2) are obtained due to the establishment of a passive behaviour above 500 mV, which indicates a direct transition from immunity region to a stable passive region (Region 2) [15].

The relatively stable current density of the alloy in NaCl was achieved in the early stage of passivation, suggesting the formation of a passive film, and then continuous oscillations of current density occurred in the range of 300–1500 mV (vs Ag/AgCl). The electrochemical parameters are listed in Table 1. From the polarization curves and the corrosion parameters listed in Table 1, it can be judged

(a) Hank's solution   **(b)** 0.9 wt.% NaCl solution   **(c)** E-MEM+10%FBS solution
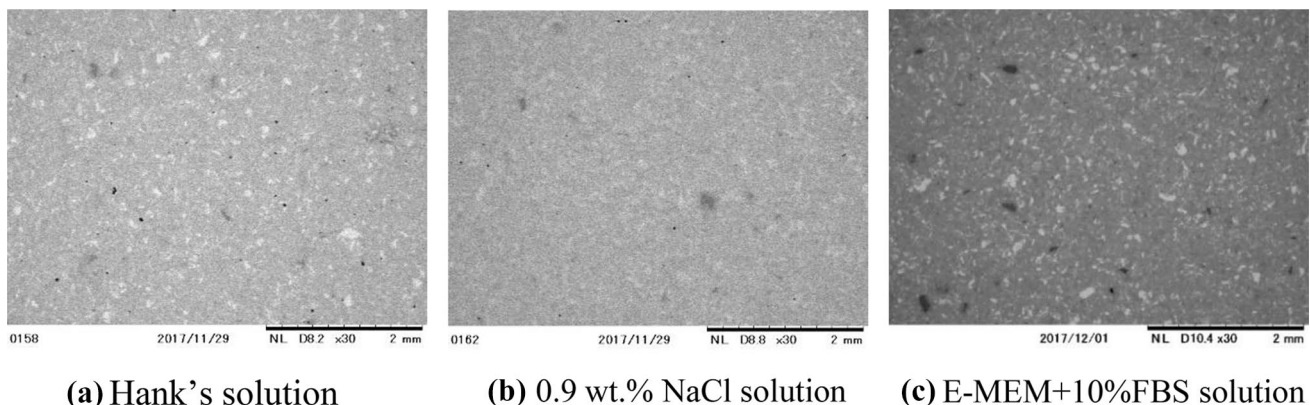
Fig. 10 Passive oxide layer in the substrates of TNZ on **a** Hank's, **b** 0.9 wt% NaCl and **c** E-MEM + 10%FBS solutions

that the comparison in three solutions shows passive state in the higher corrosion potential, lower corrosion current density, lower and more stable passive current densities and wider passive region, indicating that TNZ alloy has excellent corrosion resistance in all solutions.

4 Conclusions

According to the experimental results, the conclusion can be explained as following.

- In the current study, the sub-micron-grained TNZ alloy produced by SPS exhibited an excellent corrosion resistance, which is attributed to the formation of a thicker passive oxide film. The studied substrates showed a good corrosion performance when subjected to the simulated body fluids for a period of 4 h inside a 37 °C incubator
- The newly developed TNZ alloy substrates exhibited a complete passivation behaviour. The alloy has higher corrosion potential, lower and more stable passive current density and a wider passive region in Hank's, 0.9 wt% NaCl and E-MEM solutions, indicating that the TNZ alloy possesses much better corrosion resistance (in the range 2–4 nA/cm^2), making it a suitable candidate for biomedical applications. Corrosion resistance values for TNZ are comparable with that of Ti and Ti-64 and are published for the first time in this study.

References

1. Hussein MA, Suryanarayana C, Al-Aqeeli N (2015) Fabrication of nano-grained Ti-Nb-Zr biomaterials using spark plasma sintering. Mater Des 87:693–700
2. Hussein MA, Suryanarayana C, Arumugam MK, Al-Aqeeli N (2015) Effect of sintering parameters on microstructure, mechanical properties and electrochemical behaviour of Nb-Zr for biomedical applications. Mater Des 83:344–351
3. Mendes MWD, Agreda CG, Bressiani AHA, Bressiani JC (2016) A new titanium-based alloy Ti-27Nb-13Zr produced by powder metallurgy with biomimetic coating for use as a biomaterial. Mater Sci Eng C63:671–677
4. Niemeyer TC, Grandini CR, Pinto LMC, Angelo ACD, Schneider SG (2008) Corrosion behaviour of Ti-13Nb-13Zr alloy used as a biomaterial. Alloys Compd 476:172–175
5. Donato TAG, de Almeida LH, Nogueira RA, Niemeyer TC, Grandini CR, Caram R, Schneider SG, Santos AR Jr (2009) Cytotoxicity study of some Ti alloys used as biomaterial. Mater Sci Eng C29:1365–1369
6. Saji VS, Choe HC (2009) Electrochemical corrosion behaviour of nanotubular Ti-13Nb-13Zr alloy in Ringer's solution. Corros Sci 51:1658–1663
7. Wang YB, Zheng YF (2009) Corrosion behaviour and biocompatibility evaluation of low modulus Ti-16Nb shape memory alloy as potential biomaterial. Mater Lett 63:1293–1295
8. Arima Y, Iwata H (2007) Effects of wettability and surface functional groups on protein adsorption and cell adhesion using well-defined mixed self-assembled monolayers. Biomaterials 28:3074–3082
9. Hussein MA, Kumar M, Drew R, Al-Aqeeli N (2018) Electrochemical corrosion and in vitro bioactivity of nano-grained biomedical Ti-20Nb-13Zr in a simulated body fluid. Materials 11:1–15
10. Awang-Shri DN, Tsuchiya K, Yamamoto A (2014) Cytocompatibility evaluation and surface characterisation of TiNi deformed by high-pressure torsion. Mater Sci Eng C43:411–417
11. Suryanarayana C, Al-Aqeeli N (2013) Mechanically alloyed nanocomposites. Prog Mater Sci 58:383–502
12. Uwais ZA, Hussein MA, Samad MA, Al-Aqeeli N (2017) Surface modification of metallic biomaterial for better tribological properties: a review. Arab J Sci Eng 42:4493–4512
13. Assis S, Wolynec S, Costa I (2006) Corrosion characterization of titanium alloys by electrochemical techniques. Electrochim Acta 51(8–9):1815–1819
14. Ozan S, Lin J, Li Y, Ipek R, Wen C (2015) Development of Ti–Nb–Zr alloys with high elastic admissible strain for temporary orthopedic devices. Acta Biomater 20:176–187
15. Sowa M, Worek J, Dercz G, Korotin DM, Kukharenko AI, Kurmaev EZ, Cholakh SO, Basiagae M, Simka W (2016) Surface characterisation and corrosion behaviour of niobium treated in a Ca- and P-containing solution under sparking conditions. Electrochim Acta 198:91–103